# Western Pacific Warm Pool Region Sensitivity to Convective Triggering by Boundary Layer Thermals in the NOGAPS Atmospheric GCM

JAMES A. RIDOUT AND CAROLYN A. REYNOLDS

*Naval Research Laboratory, Monterey, California*

(Manuscript received 17 February 1997, in final form 1 August 1997)

ABSTRACT

The sensitivity of the atmospheric general circulation model of the Navy Operational Global Atmospheric Prediction System to a parameterization of convective triggering by atmospheric boundary layer thermals is investigated. The study focuses on the western Pacific warm pool region and examines the results of seasonal integrations of the model for the winter of 1987/88. A parameterization for thermal triggering of deep convection is presented that is based on a classification of the unstable boundary layer. Surface-based deep convection is allowed only for boundary layer regimes associated with the presence of thermals. The regime classification is expressed in terms of a Richardson number that reflects the relative significance of buoyancy and shear in the boundary layer. By constraining deep convection to conditions consistent with the occurrence of thermals (high buoyancy to shear ratios), there is a significant decrease in precipitation over the southern portion of the northeast trade wind zone in the tropical Pacific and along the ITCZ. This decrease in precipitation allows for an increased flux of moisture into the region south of the equator corresponding to the warmest portion of the Pacific warm pool. Improvements in the simulated distribution of precipitation, precipitable water, and low-level winds in the tropical Pacific are demonstrated. Over the western Pacific, the transition from free convective conditions associated with thermals to forced convective conditions is found to be primarily due to variations in mixed layer wind speed. Low-level winds thus play the major role in regulating the ability of thermals to initiate deep convection. The lack of coupling with the ocean in these simulations may possibly produce a distorted picture in this regard.

## 1. Introduction

A characteristic feature of the tropical western Pacific is the ''warm pool region,'' where sea surface temperatures (SSTs) are the highest in the World Ocean. Precise definitions may vary, but the SST threshold of this region is generally considered to be approximately 29°C (e.g., McPhaden and Picaut 1990). The warm pool region has received considerable attention in climate studies. It is of interest both in terms of what can be learned concerning limiting mechanisms on surface temperatures (e.g., Newell 1979; Ramanathan and Collins 1991; Waliser 1996), as well as the important effects it has on the tropical circulation (e.g., Bjerknes 1969; Huang and Sun 1992). Although generally associated with the western Pacific, the warm pool region varies in size and position, extending well into the central Pacific during the El Niño phase of the El Niño–Southern Oscillation (ENSO) (e.g., McPhaden and Picaut 1990). Despite the attention this region has received, our knowlege of it is lacking in important details, due largely to the sheer complexity of the earth's climate system. To some degree, the interaction of processes on a large range of scales, both locally and remotely, suggests the need for numerical model simulations in efforts to increase our understanding in this area. Improvements in modeling techniques and computer technology have aided in this pursuit, but numerical models remain of questionable skill in representing key processes operating in nature. In the general circulation models (GCM) used to model the large-scale circulation, errors associated with the representation of subgrid-scale phenomena such as deep convective storms, surface sensible heating, and evaporation can be substantial. Although atmospheric GCM (AGCM) results from the Atmospheric Model Intercomparison Project (AMIP) (Gates 1992) show a broad-scale agreement with major observed precipitation patterns, there are a number of regional discrepancies, including, for example, a tendency toward an unrealistic concentration of precipitation on the islands of the maritime continent during boreal winter (Lau et al. 1996). While AMIP is limited to AGCMs, troublesome systematic errors are similarly observed in coupled ocean–atmosphere model simulations (Mechoso et al. 1995).

The present study attempts to address deficiencies in the representation of boreal winter precipitation over the

*Corresponding author address:* Dr. James A. Ridout, NRL-Monterey, 7 Grace Hopper Ave., Stop 2, Monterey, CA 93943-5502.
E-mail: ridout@nrlmry.navy.mil

warm pool region in extended integrations of the AGCM of the Navy Operational Global Atmospheric Prediction System (NOGAPS) (Hogan and Rosmond 1991). During the northern winter months, NOGAPS integrations tend to exhibit a considerable underprediction of warm pool precipitation. A possible cause for this deficiency is an inadequate treatment of convective triggering in the model. Because of the important role played by boundary layer thermals in this process, a parameterization of thermal effects on convective triggering was developed and tested in the NOGAPS AGCM. The study includes an examination of the collateral roles of buoyancy and shear, which act to regulate the occurrence of thermals. By restricting the simulation tests to a single AGCM, the present study has an advantage over broader model intercomparison studies such as AMIP in that precisely defined model differences can be tested. Model sensitivity studies of this type can help to identify the significance of model changes in the context of their impact on a complex system of interacting processes. Though often difficult to interpret, such tests can be helpful in identifying which processes to emphasize in model development efforts, and can provide guidance to observational efforts for targeting specific regions or phenomena.

Considering the importance of boundary layer thermals as initiators of surface-based deep convection, it is clear that thermals have enormous implications for weather and climate. This point is of obvious importance for the problem of convective parameterization in weather and climate models, but it also indicates a very important role for processes that affect thermals in nature. The parameterization of thermal initiation of deep convection has generally not been directly addressed in GCMs, though some success has been achieved in mesoscale model studies in this regard (e.g., Kain and Fritsch 1992; Rogers and Fritsch 1996). A treatment of this issue is introduced in the present study (section 3) in the context of AGCM simulations that differs in some respects from previously described methods. Most notable perhaps is the fact that no attempt is made here to explicitly compute whether thermals can be expected to penetrate through the inversion layer under given conditions. Rather, the present treatment of convective triggering is based solely on a regime classification of the unstable boundary layer based on whether one can expect free or forced convection (or possibly some intermediate state). The cloud work function constraint in the relaxed Arakawa–Schubert (RAS) type convection scheme (Moorthi and Suarez 1992) used here, and the low-level relative humidity threshold of 50% are assumed to adequately account for additional parcel buoyancy considerations. The basis for this approach is that the boundary layer regime determines the type of large eddies that are expected in the mixed layer.

A number of AGCM simulations were carried out as sensitivity tests for the present work for the period covering December 1987 through February 1988. The results of these tests are presented in section 4, with particular attention to the warm pool region of the western Pacific. A description of the research version of the NOGAPS AGCM used for the control simulation is provided in section 2, and the parameterization for convective triggering by thermals outlined here is more fully discussed in section 3. A discussion and conclusions are given in section 5.

## 2. NOGAPS model description

The NOGAPS forecast model is used operationally by the Navy Fleet Numerical Meteorology and Oceanography Center to provide forecast guidance for navy fleet operations. In addition to its operational use, the model has been used for climate type simulations as part of AMIP. A general description of the model can be found in Hogan and Rosmond (1991) (see also Hogan and Brody 1993; Ridout et al. 1994).

For the present study, the NOGAPS forecast model was run with 18 vertical levels and a triangular truncation at wavenumber 47. As indicated above, the convective parameterization is of the relaxed Arakawa–Schubert type. Modifications have been made to the updraft model in this scheme to allow for detrainment as well as entrainment. The shallow cumulus parameterization used here differs from that in the operational version of NOGAPS in that the mixing is constrained to occur within the lowest 200 mb and cannot extend past the minimum of the boundary layer height and the cloud-base level. Clouds are parameterized essentially as described by Slingo (1987). The convective cloud fraction, however, is not allowed to exceed 0.2, and no attempt is made in the convective cloud parameterization to account for the presence of convective anvils. The radiation scheme is that of Davies (1982) and Harshvardhan et al. (1987). The boundary layer height is diagnosed following an approach similar to that of Troen and Mahrt (1986) and Holtslag et al. (1990). The scheme used for boundary layer vertical turbulent mixing is that of Louis et al. (1982). This scheme is applied above the boundary layer as well, but with the mixing coefficients reduced by a factor of 0.2. The value of this scaling parameter was chosen simply based on the results of simulation experiments with the operational version of NOGAPS (Hogan and Brody 1993). Surface fluxes were calculated based on Monin–Obukhov similarity theory following the implementation of Beljaars and Holtslag (1991). For completeness, the roughness length for momentum as a displacement height has been used, following Beljaars (1995), and the formulation for surface roughness lengths over water described in the same work has been adopted, though with a smaller coefficient in the Charnock relation (Charnock 1955) (0.011) following Smith (1980, 1988).

## 3. Parameterization for convective triggering by thermals

### *a. Basic scheme*

Because of the significance of thermals as initiators of surface-based deep convection, it can be of considerable importance to directly account for them in parameterizations of subgrid convection in numerical models. Previous treatments of the role of thermals in initiating deep convection (e.g., Kain and Fritsch 1992; Rogers and Fritsch 1996) were in mesoscale model studies in which a contribution to subgrid vertical velocity perturbations due to thermals was assumed under free convective conditions. If the parameterized vertical velocity perturbations were large enough for parcels to pass through any layer of negative buoyancy between the source level and the level of free convection, then convection was allowed. As indicated in the introduction, the treatment in the present work makes no attempt to explicitly compute whether thermals will be buoyant enough to penetrate through the inversion layer. Such a method may prove successful, but appears to be more complicated for large-scale models than for mesoscale models due to greater effects of subgrid heterogeneity. An additional consideration is the complication associated with the transition regime between free and forced convection, where the interaction of roll vortex circulations with thermals appears to be significant (Grossman 1982).

The present treatment follows a rather simple approach based on a regime classification of the unstable boundary layer. Differentiating between the regimes of free and forced convection is of primary concern here, but the potential importance of a finite transition regime between (section 3b) them is also considered. In this method, the cloud base mass fluxes predicted by the NOGAPS RAS-type convection scheme are scaled by a ''thermal growth parameter'' $t_g$ defined in section 3b. This parameter assumes the values of zero for forced convection, unity for free convection, and is scaled between these values in cases where a transition regime is considered. The boundary layer regime determines the type of large eddies that one may expect in the mixed layer. The forced convection regime is associated with the absence of thermals. It is the roll vortex circulation, rather, that tends to be the preferred mixed layer eddy in this regime. The free convection regime, on the other hand, is dominated by thermals (Grossman 1982). Clouds initiated by roll vortices appear to be trapped below the inversion level at the top of the boundary layer (e.g., LeMone and Pennell 1976; Grossman 1982), so surface-based deep convection is not expected in the forced convection regime ($t_g$ equal to zero). Cloud streets (Kuettner 1959, 1971), for example, tend to occur in this regime and generally are not associated with deep convection (Scorer 1972). There exists a potentially significant transition regime (described in section 3b) where thermals occur, but their existence appears to depend upon roll vortex circulations in which they are embedded (Grossman 1982). Previous efforts at parameterizing the effects of thermals on deep convection have not attempted to directly address this regime. Cases where deep convection develops from cloud streets (Scorer 1972) appear to be associated with this transition regime. For the present study, in simulations (section 4) where this transition regime is considered, as the limit of forced convection is approached, it is assumed that convection is reduced relative to what would occur under free convective conditions. This reduction is implemented by reducing the value of $t_g$ in this regime from its value of unity for free convection. Further discussion of this treatment is provided in the following subsections.

It is important to note that the present treatment of convective triggering by thermals is in addition to the cloud work function constraint in the RAS-type convective parameterization and a cutoff of deep convection for environments with lower than 50% relative humidity at the first model grid level. The convective parameterization assumes that updrafts associated with convective clouds originate near the surface, so the present treatment should be appropriate. For convection from elevated source levels, this proposed scheme would obviously not apply.

### *b. Unstable boundary layer regime classification*

In the preceding subsection, the effect of thermals on triggering deep convection has been described in terms of a thermal growth parameter $t_g$, defined to be unity under free convective conditions and zero for forced convection. The method used to classify these regimes in the unstable boundary layer is now described. (It should be noted that forced convection, or shear-dominated turbulence generation, occurs in the stable boundary layer as well, but the forced convection regime discussed here refers to forced convection in unstable boundary layers.) As indicated in the preceding subsection, there is some evidence (discussed below) for a clearly definable transition regime between the regimes of free and forced convection. A preliminary proposal to extend the definition of $t_g$ to treat the effects of such a finite transition regime is also presented.

The different unstable boundary layer regimes have been found in large-eddy simulation (LES) studies to be characterized by the ratio $z_i/L$ of mixed layer height to Obukhov length (e.g., Deardorff 1972). The Obukhov length is proportional to the height above the surface at which buoyancy generation of turbulence dominates over shear production of turbulence (Stull 1988), and is negative for unstable surface layers. High values of $-z_i/L$ are associated with free convection and the existence of convective cells consistent with thermals, and low values of $-z_i/L$ are associated with forced convection and in some cases the existence of roll vortices. Despite such evidence, for the present work, an alter-

native characterization of the unstable boundary layer in terms of a dimensionless ''mixed layer Richardson number'' $R_*$ (Stull 1994) was adopted. Although this choice was motivated by model performance considerations, this may simply reflect the fact that the ratio $-z_i/L$ is very sensitive to errors in the parameterization of surface drag (since the Obukhov length $L$ is proportional to the cube of the friction velocity $u_*$). The use of $R_*$ rather than $-z_i/L$ is supported in part by the fact that under free convective conditions, convective transport theory (CTT) implies (Stull 1994) that

$$-\frac{z_i}{L} = k\left(\frac{C_{*H}R_*}{C_{*D}^2}\right)^{3/4}, \tag{1}$$

where $k$ is the von Kármán constant, and $C_{*H}$ and $C_{*D}$ are transport coefficients for heat and momentum, respectively. The mixed layer Richardson number is a measure of the relative significance of buoyancy and shear in the boundary layer, and is given by

$$R_* = \left(\frac{w_{\rm B}}{U_{\rm ML}}\right)^2, \tag{2}$$

where $U_{\rm ML}$ is the mean wind speed in the mixed layer, and $w_{\rm B}$ is the ''buoyancy velocity scale'' (Stull 1994). For the present work $w_{\rm B}$ is approximated as

$$w_{\rm B} \equiv \left(\frac{g}{\overline{\theta_v}} z_i \Delta\theta_v\right)^{1/2}, \tag{3}$$

where $\overline{\theta_v}$ is the mean virtual potential temperature in the mixed layer, and the difference $\Delta\theta_v$ is taken between the surface skin and the mixed layer. Mixed layer quantities are taken as the respective mean values for model levels between $0.3h$ and $0.7h$, where $h$ is the boundary layer depth (section 2). It can be shown (Stull 1994) that $w_{\rm B}$ is proportional to the convective velocity scale $w_*$. Based on an analysis of data from the Boundary Layer Experiment—1983, Stull (1994) assumed that free convection occurs for $R_* \geq 3.0$. Further support for a transition to free convection in the neighborhood of $R_* = 3.0$ comes from data from the Barbados Oceanographic and Meteorological Experiment (BOMEX) discussed below. As we shall see, however, the BOMEX data also seem to suggest the importance of a finite transition regime between free and forced convection. Considering for a moment the case of an abrupt transition for some value of $R_*$, say $R_{*C}$, $t_g$ is given simply by

$$t_g = 1.0, \qquad R_* > R_{*C}, \quad \text{(free convection, no transition regime)} \tag{4}$$

$$t_g = 0, \qquad R_* \leq R_{*C}, \quad \text{(forced convection, no transition regime).} \tag{5}$$

Results from test simulations for different values of $R_{*C}$ are described in section 4.

In contrast to the rather simple picture of the unstable boundary layer in terms of either free or forced convection, the picture that emerged from the study of BOMEX data by Grossman (1982) included at least four different unstable boundary layer regimes. These regimes were expressed in terms of $z_{CB}/L$, where $z_{CB}$ is cloud-base height, rather than the more commonly used $z_i/L$. For the present work, it is assumed that in the trade wind cases looked at by Grossman, $z_{CB} \sim z_i$. This assumption is consistent with the study of LeMone and Pennell (1976), and its use here is consistent with the rather large uncertainty in the determination of $L$ in Grossman's study.

In one of the regimes identified by Grossman ($-z_{CB}/L \leq 5.0$), only roll vortex motion was detected. As indicated in the preceding subsection, this fact, together with the observations of LeMone and Pennell (1976), supports the present assumption that surface-based deep convection does not occur under forced convective conditions. For conditions where buoyancy was somewhat more important ($5.0 < -z_{CB}/L \leq 7.3$), convective cells (consistent with thermals) were observed, but rolls were dominant and appeared to be necessary for the maintenance of the convective cells. Grossman hypothesized that (boundary layer) convective cells in this regime tend to occur in the regions of upward motion associated with roll vortices. Thus deep convection in such an environment would tend to occur as an outgrowth from cloud streets. When cumulus clouds in cloud streets reach a certain size, however, associated downdrafts tend to destroy the cloud streets (Scorer 1972). Hence there is an apparent inconsistency between a proliferation of deep convection and the observed predominance of boundary layer roll vortex circulations in this regime. It would appear, therefore, that deep convection does not occur as readily in the trade wind environment when $-z_{CB}/L < 7.3$ as it does when $-z_{CB}/L > 7.3$, the latter regime being dominated by random convective cells (Grossman 1982). Based on these observations and the assumption that for the trade wind boundary layer upon which Grossman's study was based, $z_{CB} \sim z_i$ (see discussion above), the regime corresponding to $5.0 < -z_i/L \leq 7.3$, or some subset of this regime, is assumed here to be important as a transition regime with respect to thermal initiation of deep convection. A key factor in this respect appears to be the effect of low-level shear in reducing the strength of incipient thermal circulations, thus allowing for the dominance of roll vortices.

Although the transition regime identified in the preceding discussion was expressed in terms of $-z_i/L$, the relation (1) between $-z_i/L$ and $R_*$ was used to estimate the range of values of $R_*$ associated with this regime. Using (1) with the transfer coefficients from Stull's CTT only scheme (Stull 1994), one finds that thermals should dominate for $R_* > 4.03$ and that only roll vortices should occur for $R_* \leq 2.4$. The appropriate transition regime upper bound for the present study was taken to be $R_* = 4.0$. The lower cutoff value of $R_* = 2.4$ is very approx-

imate because CTT is not applicable for forced convection. In this regard, it is important to recognize that $R_*$ may not even be a valid classification parameter for the forced convection limit of the transition regime. Assuming that $R_*$ is in fact a valid parameter in this sense, one finds from data presented by LeMone and Pennel (1976) that a cutoff value as low as $R_* \cong 0.3$ might be justified. Based on model performance, a higher cutoff value of $R_* = 2.0$ was used for the present work. This performance-based value appears to fall somewhere within the transition regime of Grossman's study, suggesting that deep convection may not be significant for boundary layers in the more shear-dominated portion of the transition regime identified by Grossman. The thermal growth parameter $t_g$ is assumed to scale linearly with $R_*$ in the adopted transition regime, and is thus defined by

$$t_g = 1.0, \qquad R_* > R_{*C2}, \qquad \text{(free convection, finite transition regime)} \tag{6}$$

$$t_g = \frac{(R_* - R_{C1})}{(R_{*C2} - R_{*C1})}, \qquad R_{*C1} < R_* \leq R_{*C2}, \qquad \text{(transition regime)} \tag{7}$$

$$t_g = 0, \qquad R_* \leq R_{*C1}, \qquad \text{(forced convection, finite transition regime),} \tag{8}$$

where currently $R_{*C1} = 2.0$ and $R_{*C2} = 4.0$. Results from a preliminary test of this scheme are presented in section 4.

### c. Transition regime scaling

Although the treatment proposed here for free and forced convection is straightforward, the basis for the treatment in the transition regime is perhaps not as clear. The reader will recall that the parameter $t_g$ is applied to the cloud-base mass fluxes from the RAS convective scheme as a scaling factor. In the transition regime, this treatment corresponds to an increase in the adjustment timescale (by a factor of $1/t_g$), or in other words, the time required for cloud effects to reduce the cloud work function to its equilibrium value. Moorthi and Suarez (1992) found the RAS scheme to be insensitive to changes in this timescale in off-line tests. In those tests, the scheme was used to bring a sounding into adjustment with respect to a given set of cloud work function critical values. The final net temperature and moisture changes were nearly independent of the adjustment timescale that was used. However, the number of iterations required to reach the adjusted profile varied considerably. In a prognostic mode, one can expect that if the adjustment timescale is not small compared to the timescale of the large-scale forcing, then sensitivity to this parameter would be observed. In recognition of this fact, Moorthi and Suarez (1992), in a prognostic mode test using A/B-scale array data for Phase III of the GARP (Global Atmospheric Research Program) Atlantic Tropical Experiment (GATE), chose an adjustment timescale of 15 min in order to approximate results one would obtain if complete equilibrium with respect to the assumed cloud work function critical values was maintained. The results obtained in terms of the A/B-scale-averaged precipitation rates are generally quite good, though one can see from Fig. 14 of Moorthi and Suarez (1992) that perhaps 5%–10% of the time during the 18-day integration period, the observed precipitation was less than half the simulated precipitation. This occurred in spite of the fact that the large-scale forcing used was prescribed according to observations. Although inaccuracies in the data used may possibly explain the discrepancies, another possibility is that the atmosphere did not remain in equilibrium with the large-scale forcing during those periods. This would support the use of an adjustment timescale as proposed here that is not constant, or at least that is not always small compared to the large-scale forcing. The fact that during a couple of brief episodes, the observed precipitation actually vanished, whereas the simulated precipitation remained significant, supports the case for a variable adjustment timescale (in fact one that can become infinite, in agreement with the discussion in the preceding subsection concerning the implications of BOMEX observations for the forced convection regime). Further examination of Fig. 14 of Moorthi and Suarez (1992) shows episodes in which the observed precipitation was very small, but nonvanishing, whereas the simulated precipitation was fairly significant. This fact may support the use of large, but finite, adjustment timescales for certain conditions, as in the present treatment for the transition regime. However, because the A/B-scale array was fairly extensive in its spatial coverage (on the order of 7° in the zonal direction and 4° in the meridional direction), these results may simply reflect the presence of both regions of small (but finite) adjustment timescale as well as regions of infinite adjustment timescale within the A/B-scale array. Notwithstanding such uncertainties, given the present assumption that surface-based deep convection is constrained in the transition regime due to conditions in the boundary layer, the adoption of a longer adjustment timescale in that regime than for free convection seems reasonable.

TABLE 1. Summary of primary model runs discussed in the text.

| Experiment | Description |
|---|---|
| CTL | Control |
| EX1 | Modified convective trigger, transition regime ($2.0 \leq R_* \leq 4.0$) |
| EX2 | Modified convective trigger, transition at $R_* = 1.0$ |
| EX3 | Modified convective trigger, transition at $R_* = 2.0$ |
| EX4 | Modified convective trigger, transition at $R_* = 3.0$ |
| EX5 | Modified convective trigger, transition at $R_* = 5.0$ |
| EX6 | Same as CTL, but relative humidity threshold $rh_c = 0.84$ |
| EX7 | Same as CTL, but relative humidity threshold $rh_c = 0.86$ |
| EX8 | Same as CTL, but relative humidity threshold $rh_c = 0.88$ |
| EX9 | Same as CTL, but relative humidity threshold $rh_c = 0.90$ |

## 4. Model sensitivity to thermal triggering of deep convection

### *a. Preliminary comparisons*

A preliminary examination of NOGAPS sensitivity to the convective triggering parameterization described in the preceding section was carried out by means of extended model integrations using observed monthly mean SSTs linearly interpolated to the model time step for the period covering November 1987–February 1988. For each model version tested, three simulations were run starting from different initial conditions. The initial conditions were obtained from a simulation with a model version similar to that described in section 2. There was a four day temporal separation between the initial conditions used for each of the three ensemble members for each experiment, though the simulations were all started from 1 November 1987. A 1-month spinup period was allowed, and ensemble 3-month mean results are presented here for December–February (DJF). The control simulation (CTL) used for these tests was carried out using the model briefly described in section 2. The first experimental simulation (EX1) discussed here was run assuming the finite boundary layer transition regime given by (6)–(8) with $R_{*C1} = 2.0$ and $R_{*C2} = 4.0$. A summary description of these simulations and others in this section is given in Table 1. It should be noted that the use of relatively small (three-member) ensembles in this subsection represents an attempt to accomodate a greater number of sensitivity tests. Comparison of results shown here for the three-member CTL and EX1 ensembles with results from corresponding five-member ensembles discussed in section 4b suggests that three-member ensembles are sufficiently robust for the present comparisons.

The precipitation fields produced in the simulations are of interest because they provide a picture of important features of the general circulation such as the intertropical convergence zone (ITCZ), the South Pacific convergence zone, and midlatitude storm tracks. As a measure of the actual precipitation that occurred during the simulation time period, precipitation fields based on observations produced as part of the Global Energy and Water Cycle Experiment (GEWEX) of the World Climate Research Program were used. The GEWEX dataset is based on a blend of fields from gauge data, satellite microwave and infrared retrievals, and in data-sparse regions, forecast fields from the European Centre for Medium-Range Weather Forecasts (ECMWF).

The DJF mean precipitation rate ''observations'' and simulation ensemble results from CTL and EX1 are shown in Fig. 1. Both ensembles reproduce the general features of the GEWEX precipitation distribution, though they tend to predict too much precipitation in the western Indian Ocean and too little in the maritime continent. The control ensemble tends to overpredict rainfall over certain continental regions by a substantial amount. The modified trigger function (EX1) has a significant positive impact in this regard in South America and the southern half of Africa, though rainfall over the latter region is overpredicted in both ensembles. There is a substantial overprediction of precipitation in CTL in the western Pacific Ocean along the ITCZ and in the northeast trade wind region. The excessive precipitation in those regions is accompanied by an underprediction over the very warm waters that exist in the tropical western Pacific to the south of the equator. This underprediction of warm pool precipitation in CTL and the differences between CTL and EX1 are more clearly evident in the ''error'' plots shown in Fig. 2, constructed by computing the differences between the simulation results and the GEWEX precipitation rates. The boxed region (bounded latitudinally by 15°S and 0° and longitudinally by 160°E and 165°W) corresponds roughly with the region of warm pool precipitation deficit in CTL. As shown in Fig. 3, the boxed region falls generally within the 29°C SST isotherm. For reference purposes, this region will be referred to here as the ''warm pool RD'' (rainfall deficit) region. This region will be the focus of further analysis in the following subsection. For the present, note that although in EX1 there is some tendency toward an overcorrection of the precipitation deficit in the warm pool RD region seen in CTL, the results obtained for EX1 in the western Pacific are generally considerably better than for CTL. The overprediction of precipitation in the western Indian Ocean in EX1 may reflect a need to assess the ability of thermals to penetrate the inversion at the top of the boundary layer. As shown below, other more ad hoc treatments can also be effective in correcting this problem. The precipitation deficit over the Maritime Continent obtained for both ensembles may possibly be due to spectral truncation errors associated with the large horizontal gradients in terrain height in that region.

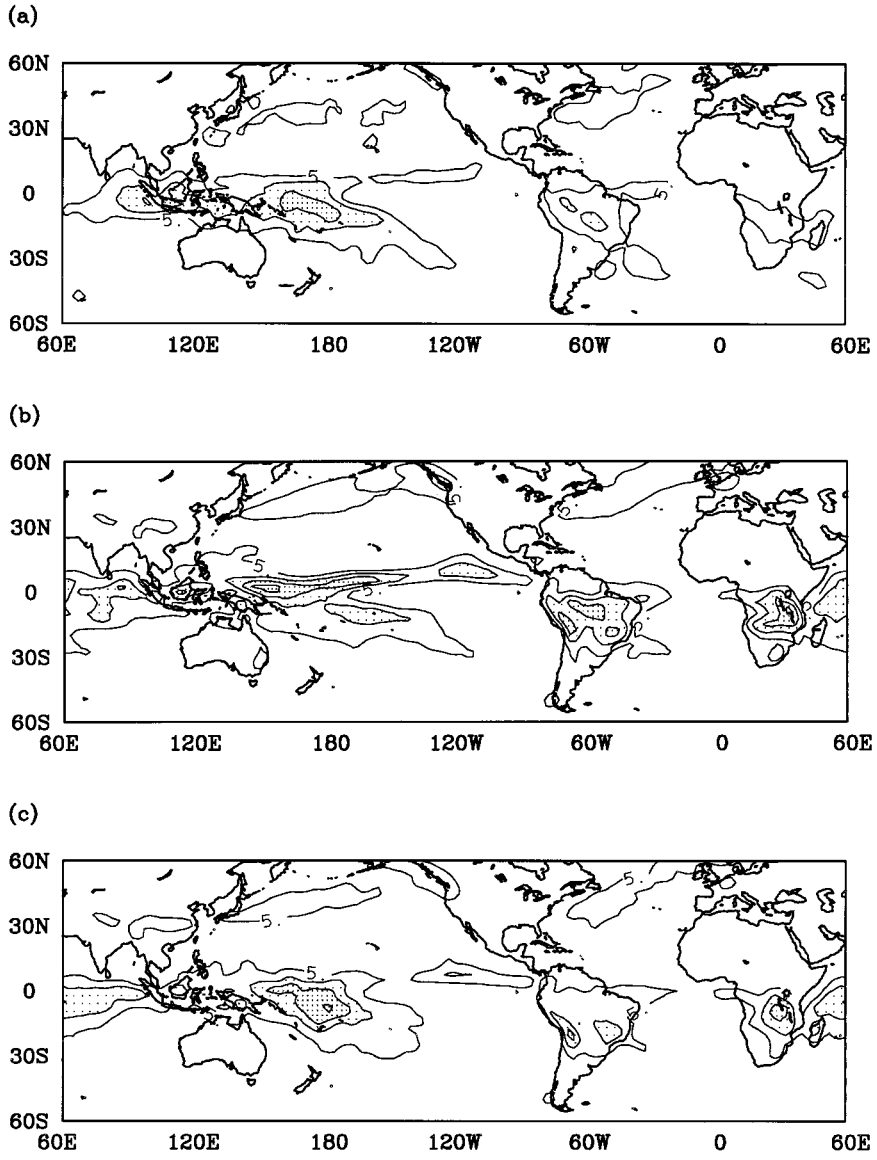


FIG. 1. Three-member ensemble DJF mean surface precipitation rate (mm day$^{-1}$): (a) GEWEX data, (b) CTL, and (c) EX1. Contour interval 5 mm day$^{-1}$. Minimum contour 5 mm day$^{-1}$.

To further examine the sensitivity of simulated precipitation fields to the convective triggering parameterization of section 3, the DJF mean precipitation rate is shown in Fig. 4 for four ensembles EX2–EX5. These ensembles are identical to EX1 except that an abrupt transition [(4) and (5)] is assumed from free to forced convection. The transition point $R_{*C}$ used in these ensembles varied from 1.0 in EX2 to 5.0 in EX5 (Table 1). The results reveal a progressively weaker ITCZ in the eastern Pacific as $R_{*C}$ is increased, becoming somewhat poorly defined in the extreme case of $R_{*C} = 5.0$. Precipitation over South America also decreases with increasing $R_{*C}$. On the other hand, calculations show that precipitation over the warm pool RD region increases as $R_{*C}$ increases, exceeding the observed rainfall in EX3–EX5. It appears from the results shown that the optimal transition point in NOGAPS lies somewhere between $R_{*C} = 2.0$ and $R_{*C} = 5.0$, perhaps in the neighborhood of $R_{*C} = 3.0$. This result lends some indirect support to the general thesis underlying the present parameterization in its consistency with expectations based on BLX83 and BOMEX data, as discussed in the preceding section.

Consistent with the discussion in section 3, it is not difficult to show that the case $R_{*C} = 2.0$ (EX3) and the finite transition regime case treated in EX1 differ only in terms of a finite scaling of the adjustment timescale of the RAS convective parameterization in the transition regime selected for EX1. Comparison of Fig. 4b with Fig. 1c shows significant differences between the two

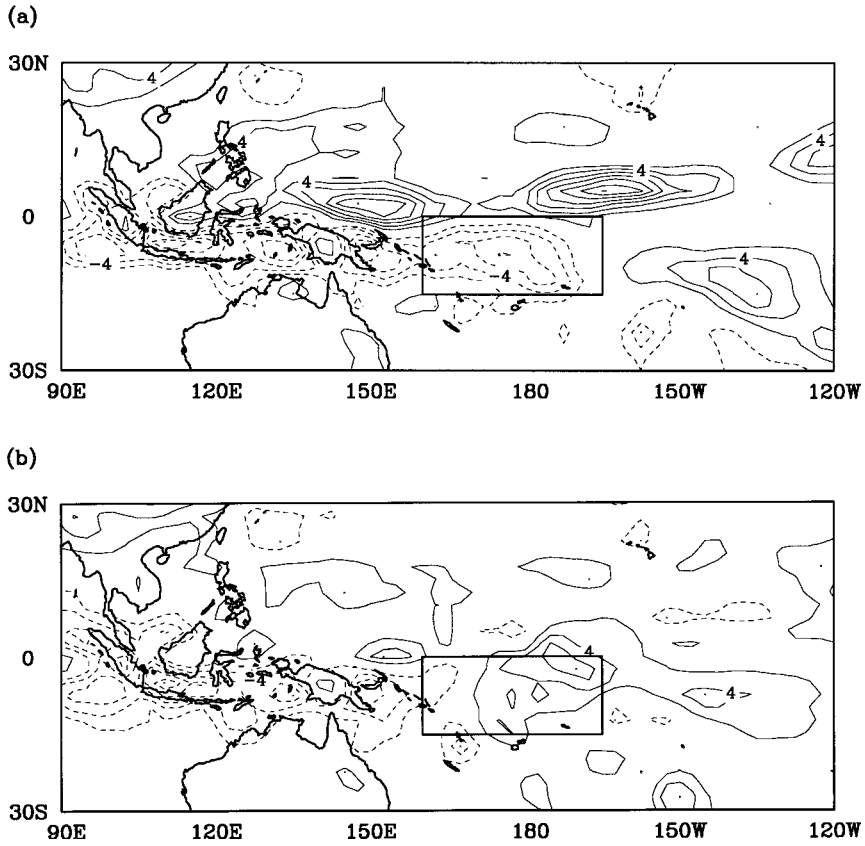


FIG. 2. Three-member ensemble DJF mean surface precipitation rate error based on GEWEX data (mm day$^{-1}$): (a) CTL and (b) EX1. Contour interval 2 mm day$^{-1}$. Zero contour omitted. Dashed lines indicate negative values.

ensembles, illustrating the impact of the treatment in the transition regime. The differences suggest that the effective adjustment timescale in EX1 (taking into account the scaling of the cloud base mass fluxes by $t_g$) is often significant with respect to the timescale of the large-scale forcing.

Some preliminary tests were carried out using a version of NOGAPS in which the convection scheme was shut off entirely, corresponding to the limit as $R_{*C}$ approaches infinity. The results obtained (not shown) show an excessive amount of warm pool precipitation due to large-scale vertical uplift over the western Pacific. This uplift results from buoyancy created by the mixing of warm, moist air from the surface over the warm pool. To verify this point, tests were also run using zonally constant SSTs, showing no such concentration of precipitation in the western Pacific. Given this tendency for precipitation over the warm pool region, even apart from the effects of deep convection, it appears that simulated precipitation deficits over the warm pool cannot

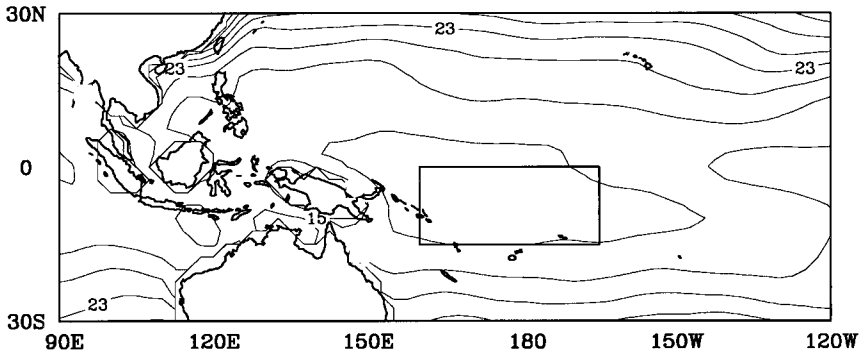


FIG. 3. Mean DJF SSTs (°C). Contour interval 2°C.

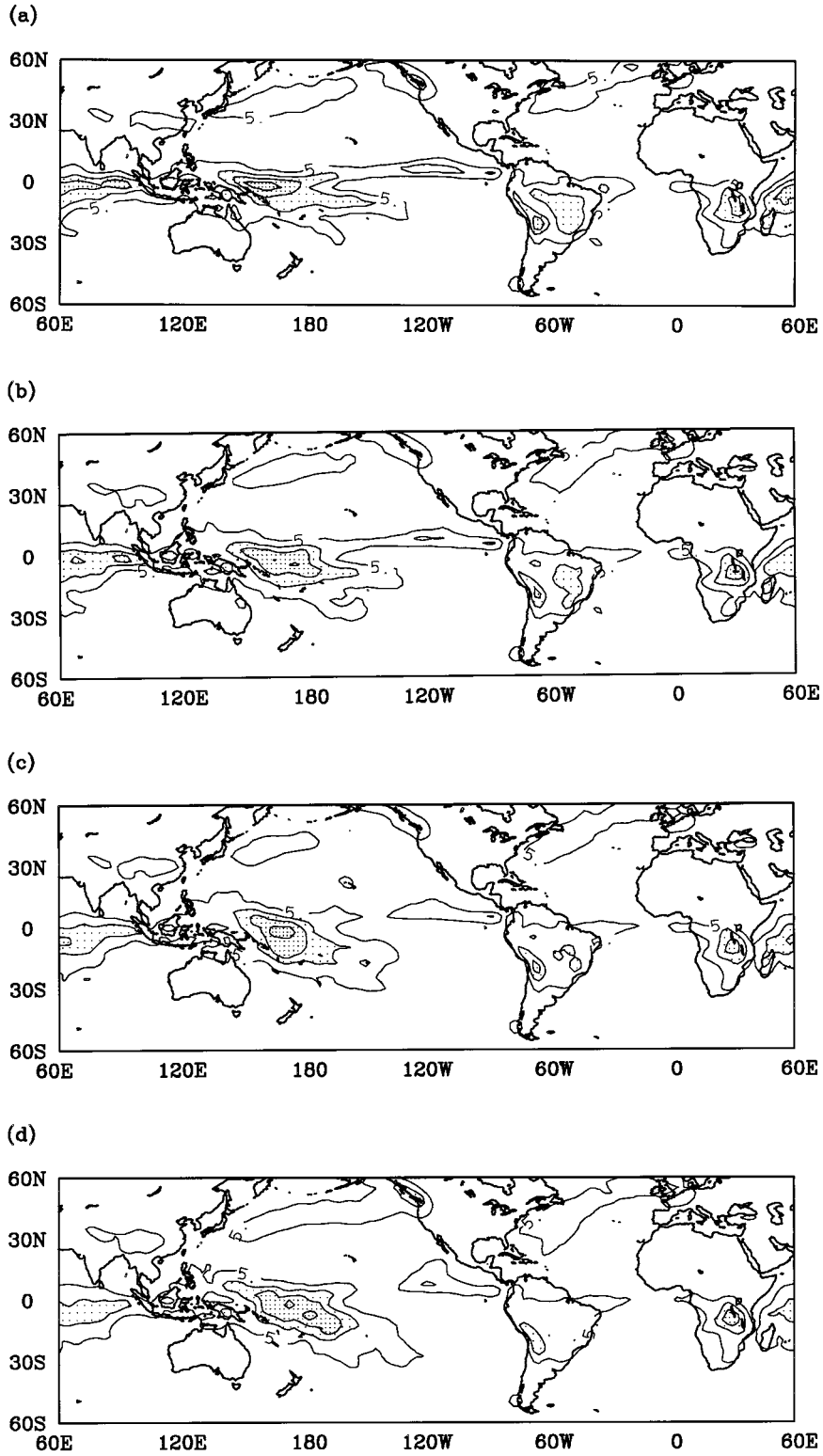


FIG. 4. Three-member ensemble DJF mean surface precipitation rate (mm day$^{-1}$): (a) EX2, (b) EX3, (c) EX4, and (d) EX5. Contour interval 5 mm day$^{-1}$. Minimum contour 5 mm day$^{-1}$.

necessarily be attributed to insufficient convection over the region. One mechanism that can possibly lead to unrealistically low amounts of warm pool precipitation, however, is dynamical suppression of low-level convergence over the warm pool due to the occurrence of an excessive amount of deep convection nearby. Examination of Fig. 1 suggests that suppression of this nature may be occurring in CTL due to the excessive convection in that ensemble along the ITCZ. This observation suggests that a convective parameterization that sufficiently reduces convection along the ITCZ should produce adequate amounts of warm pool precipitation. One method of accomplishing this is simply to raise the low-level relative humidity threshold for convection $rh_c$ to a high enough level. To compare this treatment with the present scheme, four three-member simulation ensembles (EX6, EX7, EX8, and EX9) were constructed that are identical to CTL except that $rh_c$ was set at 0.84, 0.86, 0.88, and 0.90, respectively. The mean DJF precipitation distributions obtained are shown in Fig. 5, and the errors are shown in Fig. 6. These plots reveal a high amount of sensitivity to the relative humidity threshold. As the threshold is raised, the amount of rainfall over the warm pool increases, and precipitation decreases along the ITCZ in the central and eastern Pacifc. The optimal value, based on warm pool precipitation, appears to be approximately 0.86. Although the amount of warm pool precipitation can apparently be adjusted in this manner, the precipitation distribution obtained using the boundary layer regime based trigger (Fig. 1c) generally appears more realistic. An exception is the western Indian Ocean, where the elevation of $rh_c$ from the value of 0.5 used in CTL has considerably reduced the amount of excess precipitation. The fact that this improvement occurs even for the lowest value of $rh_c$ tested suggests that a temporary solution to the overprediction of rainfall in the western Indian Ocean in EX1 may be to raise $rh_c$ to some intermediate value.

A final point regarding the relative humidity threshold convective trigger concerns the apparent tendency toward overprediction of precipitation over the islands of the Maritime Continent for certain values of $rh_c$. This is particularly evident for $rh_c = 0.84$ (Fig. 6a). One finds in Fig. 6 that the problem tends to diminish somewhat for larger threshold relative humidities. This phenomenon, a common problem in GCM simulations (Lau et al. 1996), does not occur when the convective trigger of section 3 is used (Fig. 2b). Preliminary tests with NOGAPS suggest that this problem might be more serious in models in which a convective adjustment scheme is called after the deep convective parameterization (in this case RAS) scheme is called. In NOGAPS, such a treatment results in a lower optimal value of $rh_c$ (approximately 0.82 based on simulated warm pool precipitation), and a precipitation excess over the islands of the Maritime Continent much the same as in Fig. 6a.

### *b. Warm pool region*

As we have already seen, the increased precipitation over the warm pool RD region (boxed region in Fig. 2) appears to be connected with the concommitant reduction seen in precipitation to the north of the equator along the ITCZ and in the northeast trade wind zone. In the present subsection, a somewhat more detailed investigation is made of the response of the warm pool region to the present parameterization. The investigation focuses primarily on the case of the finite transition regime (EX1). To help ensure the statistical significance of the results shown, two more simulations were carried out for the EX1 and CTL ensembles for this subsection. The initial conditions used for the two additional ensemble members corresponded to the midway point between the initial conditions used for the simulations described above. The mean DJF precipitation fields from these ensembles are shown in Fig. 7, along with the difference field between EX1 and CTL. Shading is used in Fig. 7c to indicate where the Student's t-test assigns a statistical significance to the difference between the precipitation rates for CTL and those for EX1, scaled with the pooled intersimulation variability of those errors, at the 95% level. The reader will note the considerable similarity between Figs. 7a and 7b and Figs. 2a and 2b. This similarity lends support to the statistical significance of the results from the preceding subsection. The disparate response of the northeast trade wind and warm pool RD regions to the new convective trigger is clearly evident in Fig. 7c. In addition to the reduction in precipitation in the northeast trade wind zone in EX1, the amount of precipitation is also reduced in the southeast trade wind zone in the eastern South Pacific.

A look at the vertically integrated moisture fluxes for CTL and EX1 (Fig. 8) gives some additional insight into the effect of the convective trigger modification. One finds that the increased precipitation over the warm pool RD region in EX1 can be attributed largely to an increased flux of moisture into the region from the west and from the north. The results of a moisture budget calculation are shown in Table 2 expressed in terms of corresponding rates of change in the vertically integrated moisture over the region. Inspection shows that although there was a substantial increase in moisture flux from the west and north, the moisture flux from the east is little changed. There is an increase in surface evaporation that is due to an increase in the mean low-level wind speed (not shown) over the region. In Fig. 9, the difference between evaporation and precipitation is plotted for the two ensembles. In both cases, there are extensive regions where evaporation exceeds precipitation in the northeast and southeast trade wind zones, which are thus significant sources of atmospheric moisture. In contrast, the region along the ITCZ just to the north of the equator has more precipitation than evaporation for both ensembles. The magnitude of this difference is considerably greater for CTL, which thus

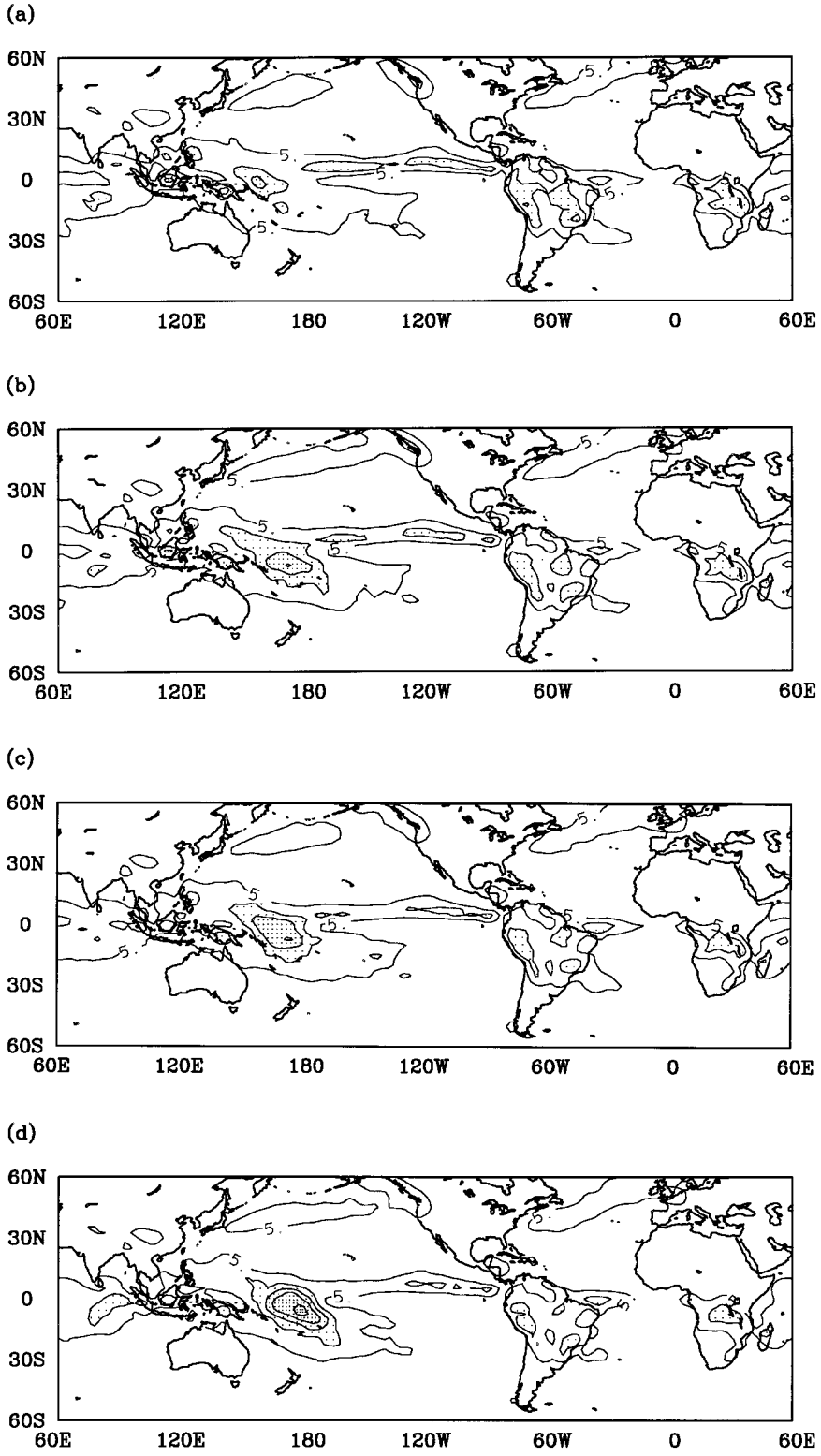


FIG. 5. Three-member ensemble DJF mean surface precipitation rate (mm day$^{-1}$): (a) EX6, (b) EX7, (c) EX8, and (d) EX9. Contour interval 5 mm day$^{-1}$. Minimum contour 5 mm day$^{-1}$.

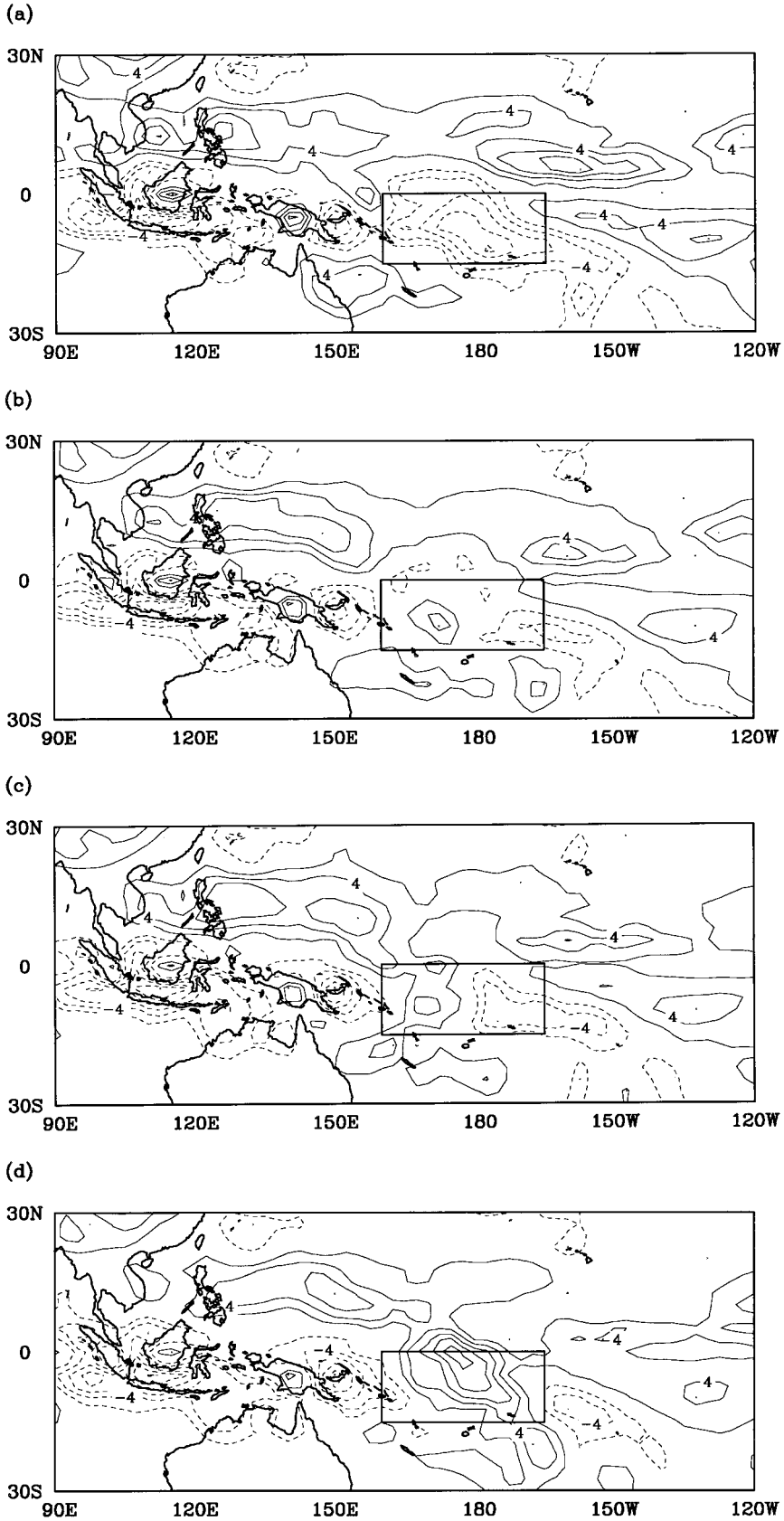

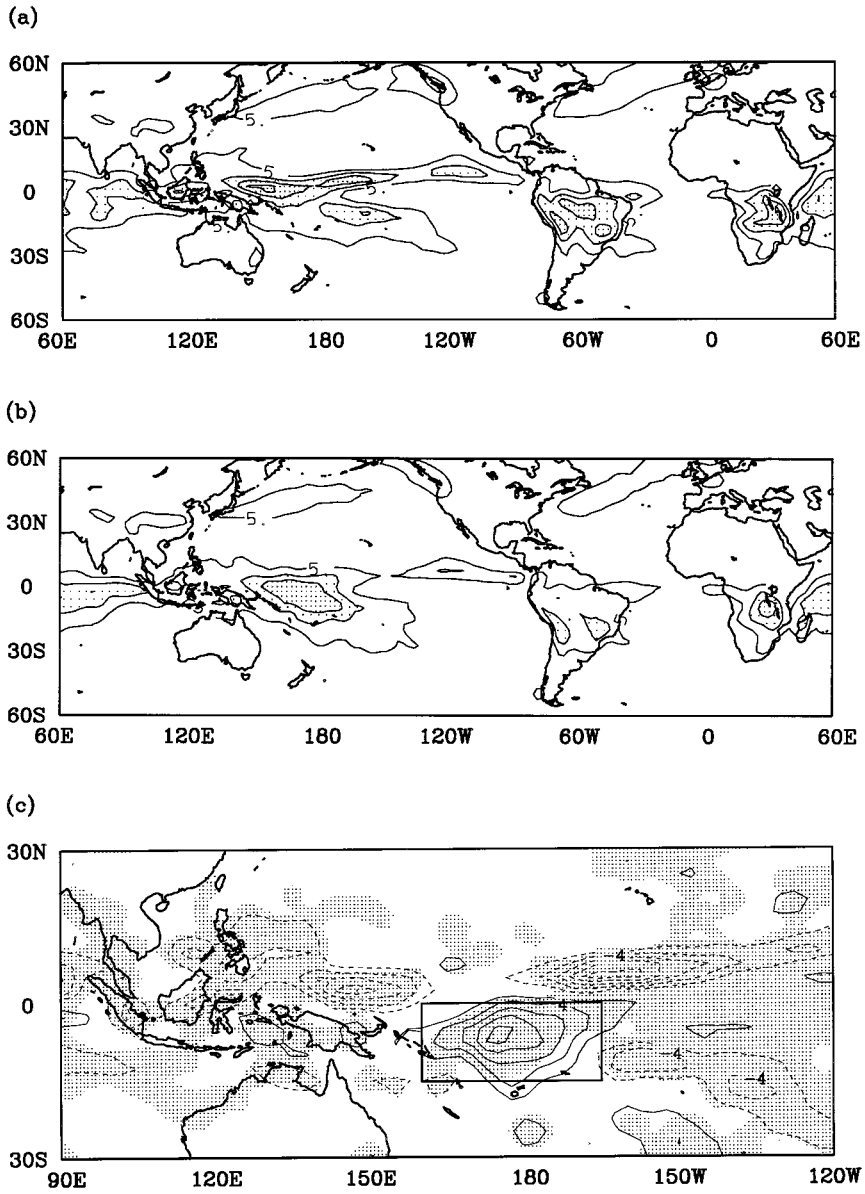


FIG. 7. Five-member ensemble DJF mean surface precipitation rate (mm day$^{-1}$): (a) CTL and (b) EX1. Contour interval 5 mm day$^{-1}$. Minimum contour 5 mm day$^{-1}$. (c) Mean DJF difference in surface precipitation rate (mm day$^{-1}$) between EX1 and CTL. Contour interval 2 mm day$^{-1}$. Zero contour omitted. Dashed lines indicate negative values. Shading indicates statistical significance of differences at the 95% level based on a Student's t-test.

has a greater net moisture loss to the surface in that region. These results are consistent with the precipitation differences plotted in Fig. 7. If one compares the moisture fluxes in Fig. 8b with the change in net moisture source from the surface plotted in Fig. 9c, one finds that the regions of reduced net moisture loss to the surface to the north of the equator in EX1 lie directly upstream of the warm pool RD region (to the north and to the west). On the other hand, the reduction in moisture loss to the surface to the east of the warm pool RD region in EX1 does not appear to affect moisture fluxes into the region from the east to any considerable extent

←

FIG. 6. Three-member ensemble DJF mean surface precipitation rate error based on GEWEX data (mm day$^{-1}$): (a) EX6, (b) EX7, (c) EX8, and (d) EX9. Contour interval 2 mm day$^{-1}$. Zero contour omitted. Dashed lines indicate negative values.

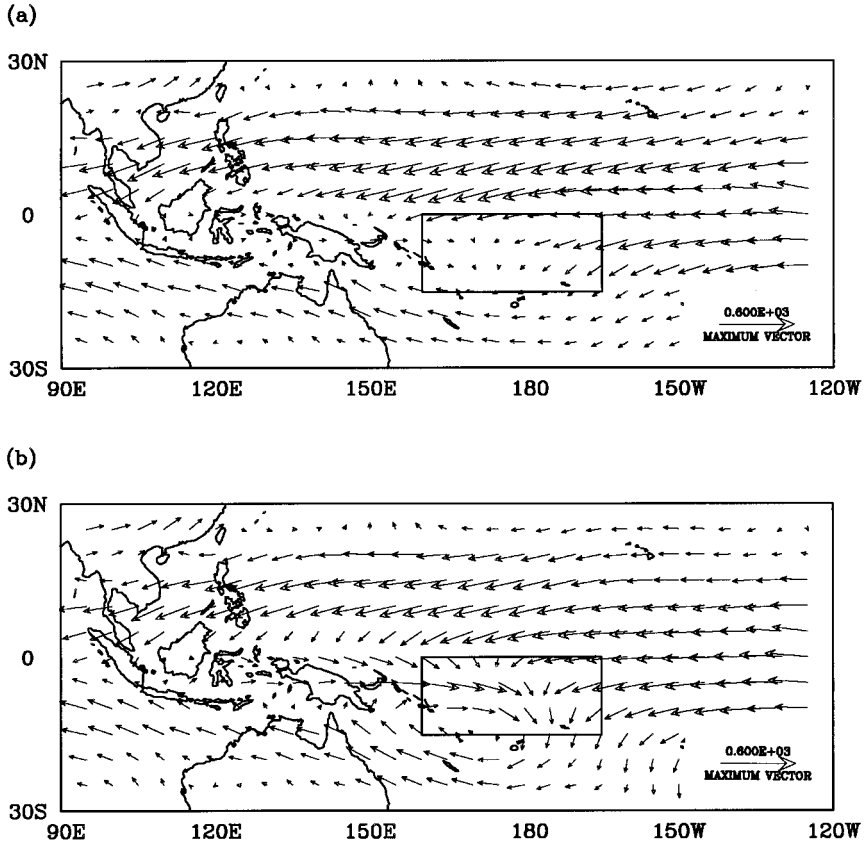


FIG. 8. Five-member ensemble DJF mean vertically integrated moisture flux (kg $m^{-1}$ $s^{-1}$): (a) CTL and (b) EX1.

due to the southerly component to the flow. This is consistent with the results shown in Table 2. The increased moisture fluxes into the warm pool RD region are apparently caused primarily by a combination of reduced moisture loss to the surface and a change in the large-scale flow, both due to a reduction in deep convection in the northeast trade wind zone and along the ITCZ. The tendency for deep convection to occur to an unrealistic extent in the northeast trade wind zone in CTL can apparently be attributed to the extension well to the north of the equator of relatively high SSTs in the tropical Pacific (Fig. 3) combined with the lack of a treatment for suppression of deep convection due to low-level shear.

TABLE 2. Simulated ensemble mean DJF water budget for the warm pool RD region (boxed region in Fig. 2) from CTL and EX1. All figures are given in terms of the equivalent rate of change in mm $day^{-1}$ of the vertically integrated moisture over the region.

| Moisture source or sink | CTL | EX1 |
|---|---|---|
| Precipitation | −10.2 | −13.9 |
| Evaporation | 5.9 | 6.6 |
| Net flux from the west | −0.0 | 2.9 |
| Net flux from the east | 3.5 | 3.9 |
| Net flux from the north | 2.0 | 3.2 |
| Net flux from the south | −0.4 | −1.7 |

That EX1 represents a reasonable picture of the seasonal mean circulation over the warm pool RD region is supported by plots of 1000-mb wind field errors based on the ECMWF analysis (Fig. 10). There is an increase in the strength of the westerlies in the tropical Pacific in EX1, and an enhancement of the flow across the equator from the north that are generally in agreement with the analyzed winds. However, there is evidence that the mass flux convergence into the warm pool RD region may be somewhat too strong in EX1. This would be consistent with the fact that the mean precipitation rate in the region for EX1 of 13.9 mm $day^{-1}$ (Table 2) is somewhat greater than the 12.5 mm $day^{-1}$ observed (GEWEX). On the other hand, the mean rate of 10.2 mm $day^{-1}$ for CTL appears to be too low. Comparison of the simulated mean precipitable water amounts for January and February with amounts based on a retrieval from Special Sensor Microwave/Imager (SSMI/I) data (Fig. 11) also show a general improvement for EX1. The greater amount of atmospheric moisture in this ensemble is consistent with the reduced moisture loss to the surface upstream of the warm pool RD region as

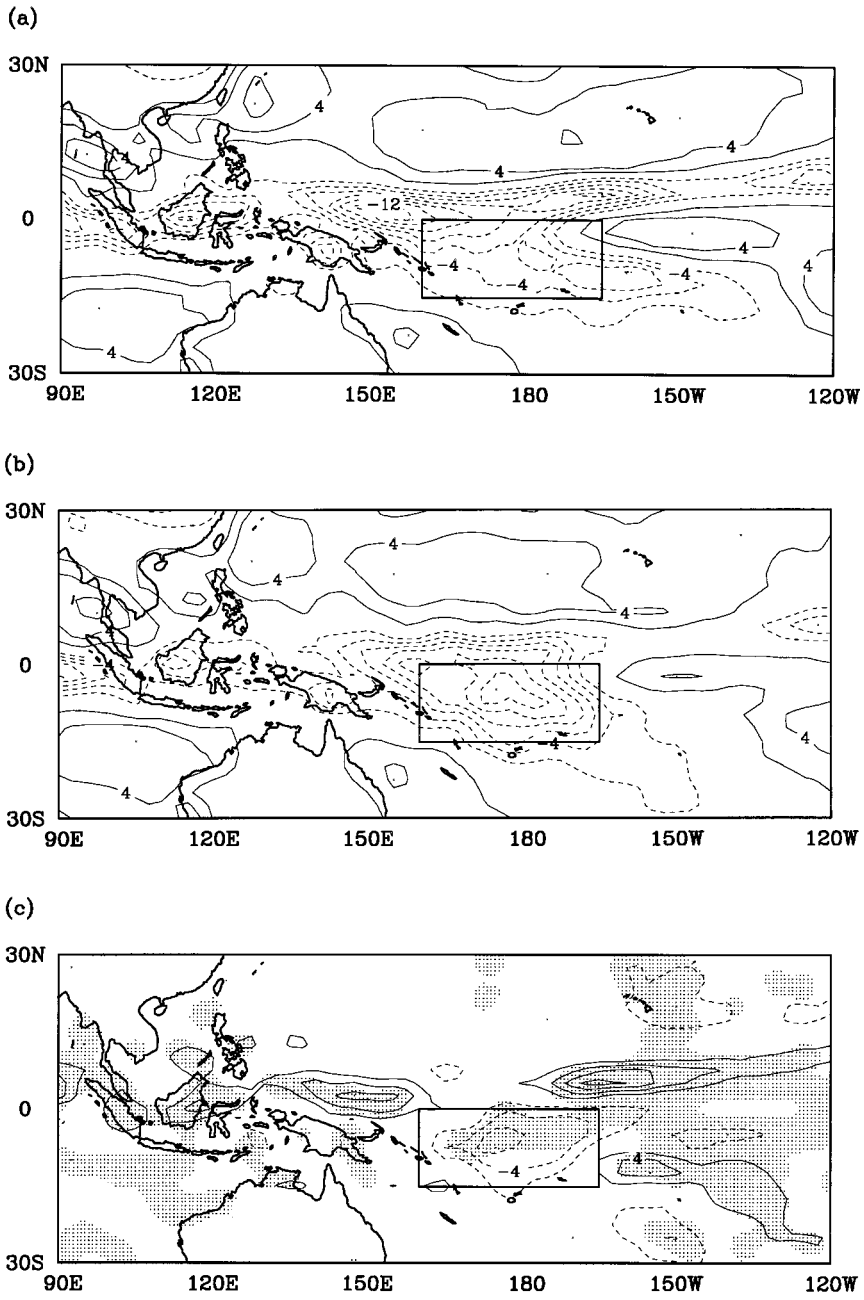


FIG. 9. Five-member ensemble DJF mean difference between evaporation and precipitation rate (mm day$^{-1}$): (a) CTL, (b) EX1, and (c) EX1–CTL. Contour interval 2 mm day$^{-1}$. Zero contour omitted. Dashed lines indicate negative values. Shading is defined as in Fig. 7.

well as the greater low-level mass convergence into that region that we have seen.

A point of some concern in this study was the fact that the warm pool precipitation in EX1 is largely due to large-scale condensation. Only 33% of the precipitation over the warm pool RD region in EX1 is convective rainfall. On the other hand, almost all of the rainfall in CTL over that region is convective. Observations for the portion of the western Pacific from 15°S to 15°N and from 130°E to 180° during the period from November 1992 through February 1993 reported in a study by Liu et al. (1995) suggest that the proportion of convective rainfall was approximately 64%. Over this larger region, the fractional amount of convective rainfall in CTL and EX1 was 100% and 43%, respectively. One explanation is that the trigger function employed here is too restrictive. The present scheme does not account, for example, for subgrid variability that could

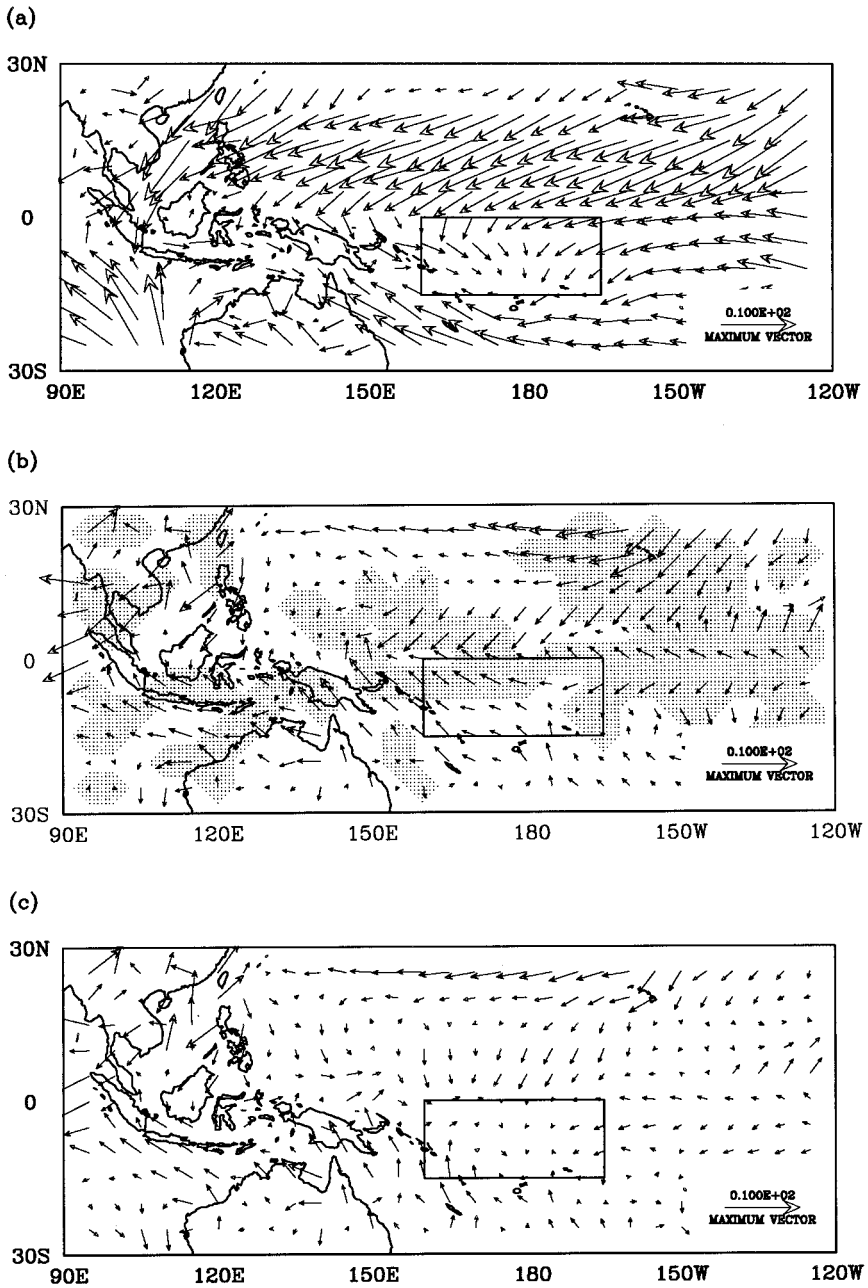


FIG. 10. (a) Mean DJF 1000-mb wind field (m $s^{-1}$) from ECMWF analysis. (b) Five-member ensemble DJF mean 1000-mb wind field error (m $s^{-1}$) for CTL based on ECMWF analysis; (c) same as (b) but for EX1. Shading is defined as in Fig. 7 but refers here to the significance of the differences in the magnitudes of the wind errors.

have a substantial impact on the initiation of convection (Rogers and Fritsch 1996). Another explanation is that the apparent deficiency results from the lack of a treatment for convection from elevated source levels, which is common in areas of strong horizontal convergence. Preliminary tests show that the apparent deficiency in convective precipitation in the western Pacific is eliminated when a simple entraining plume model is used in place of the entraining/detraining updraft model used in the RAS scheme employed in this study. By modifying the assumed precipitation efficiencies, one can obtain a precipitation distribution similar to that of EX1 (Fig. 7b), except that the magnitudes over the warm pool region err even more on the high side. This result may suggest that the present convective scheme does not respond adequately to the large-scale forcing present over the warm pool region. Nonetheless, because of the large-scale uplift over the warm pool, moisture advected

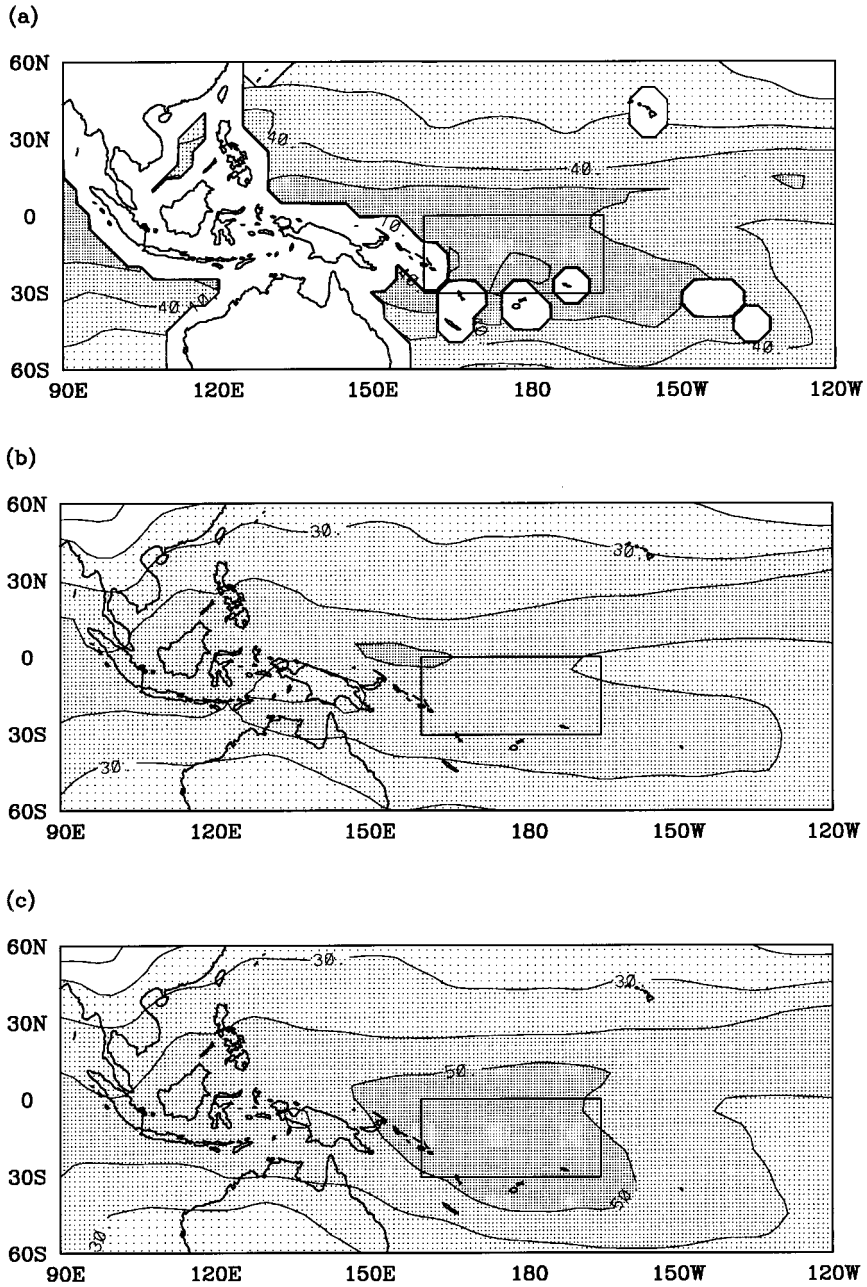


FIG. 11. (a) DJF mean precipitable water (mm) based on SSMI data. (b) Five-member ensemble DJF mean precipitable water amount (mm) for CTL. (c) Same as (b) but for EX1. Contour interval 10 mm.

into the region or evaporated from the sea surface there tends to eventually precipitate out. The profile of total heating rate due to diabatic processes and vertical eddy mixing, the so-called apparent heat source (Yanai et al. 1973), for CTL and EX1 over the warm pool RD region (Fig. 12) shows that despite concerns of too little convective rainfall, the profile for EX1 has a substantial peak at approximately the 400–500-mb level, in general agreement with observations in the western Pacific Ocean (Webster and Lucas 1992).

To better understand the regional implications of the boundary layer regime–based convective triggering parameterization described here, the DJF mean distribution of the thermal growth parameter $t_g$ defined in (6)–(8) is shown for EX1 in Fig. 13. This parameter, it should be recalled, is unity for free convection and zero for forced convection. In EX1, a finite transition regime was assumed, so $t_g$ could also assume values between zero and one. As one can see from the definition of $t_g$, the plotted values represent the net outcome of com-

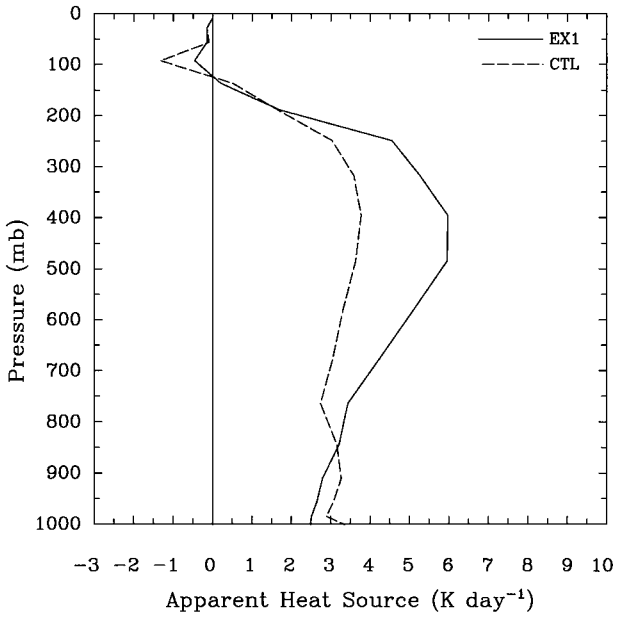


FIG. 12. Five-member ensemble DJF mean apparent sensible heat source profile for CTL and EX1.

peting effects of low-level buoyancy and shear. Although one does see smaller values in the Pacific northeast trade wind zone than in the warm pool region, the magnitude of $t_g$ over the warm pool is not particularly large, being in the range from 0.1 to 0.2. In contrast, values in the range from 0.3 to 0.4 are not uncommon. Over some near-coastal ocean waters, this is apparently due to the flow of relatively cold continental air over the warmer sea surface. Examples include the regions over the Kuroshio Current off the coasts of China and Japan, and off the east coast of the United States over the Gulf Stream.

The mean values of $t_g$ in Fig. 13 are generally strongly correlated with the fractional time during which the boundary layer is in a state of free convection. For the warm pool RD region, the boundary layer in EX1 is unstable for 99% of the time. The fractional time of free convection is 0.12, whereas the fractional time of forced convection is 0.77. Based on the present convective trigger parameterization, therefore, surface-based deep convection can potentially occur approximately 25% of the time, though almost half of this time corresponds to the transition regime between free and forced convection. If one looks at the equal-area region just to the north of the warm pool RD region (from 0° to 15°N and 160°E to 165°W, and referred to here as the northeast trade wind region), again the boundary layer is unstable 99% of the time. The fractional times of free convection and forced convection are 0.04 and 0.92, respectively. The transition from free convection to forced convection over these regions in EX1 is controlled primarily by variations in the mixed layer wind speed. Recalling the boundary layer regime description given by (2) and (6)–(8), this fact is evident from Table 3, where the DJF mean values of the buoyancy velocity scale $w_B$ and the mixed layer wind speed $U_{ML}$ for both free and forced convective conditions are shown for the warm pool RD region and the northeast trade wind region. Whereas the mean values of $w_B$ differ by no more than 50%, the mean mixed layer wind speeds are approximately a factor of 4 greater in the forced convection regime than in the free convection regime. The results differ little between the warm pool RD region and the northeast trade wind region. A reason why this may not be an accurate reflection of the relative significance of buoyancy and shear variability for western Pacific boundary layer regime determination is reviewed in section 5, suggesting the need for further study.

TABLE 3. EX1 DJF ensemble mean values of $w_B$ and $U_{ML}$ for the free and forced convection regimes for the warm pool RD and northeast trade wind regions defined in the text.

| | Free convection | | Forced convection | |
|---|---|---|---|---|
| | Warm pool RD region | Northeast trade wind | Warm pool RD region | Northeast trade wind |
| $w_B$ (m s$^{-1}$) | 8.08 | 7.95 | 5.94 | 5.35 |
| $U_{ML}$ (m s$^{-1}$) | 2.72 | 2.74 | 10.80 | 12.79 |

## 5. Discussion and conclusions

A parameterization for thermal triggering of surface-based deep convection has been presented that is based

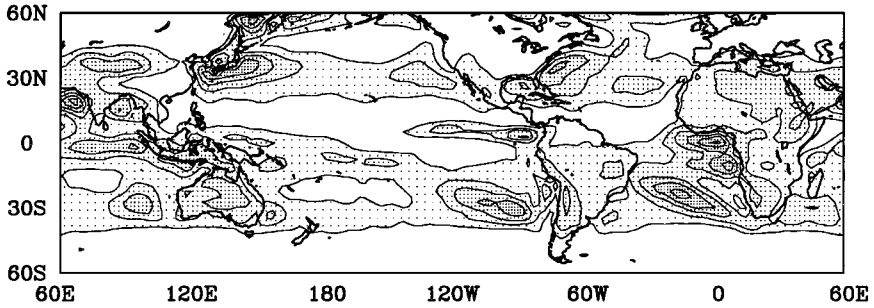


FIG. 13. Five-member ensemble DJF mean value of the "thermal growth" parameter $t_g$. Contour interval 0.1. Minimum contour 0.1.

on the boundary layer regime dependence of thermal circulations observed during BOMEX (Grossman 1982). By means of extended model integrations with prescribed SSTs, some preliminary investigations of the sensitivity of the NOGAPS AGCM to this parameterization have been made, with an emphasis on the significant effects it has on the western Pacific warm pool region. The most significant impact of the parameterization on that region occurs indirectly by means of a suppression of convection to the north in the northeast trade wind zone and along the ITCZ. As a consequence of this suppression, there is a considerable increase in low-level convergence over the warm pool region, and hence of precipitation. Comparison of simulated precipitation, precipitable water, and low-level winds with observed and analyzed fields show that the new parameterization results in a general improvement over the tropical Pacific.

Although not a focus of this study, the present convective trigger parameterization has a substantial impact on precipitation over South America, where it acts to significantly reduce precipitation, resulting in better agreement with observations. A considerable overprediction of rainfall in NOGAPS over the western Indian Ocean is not corrected by the new scheme. This may reflect a need to assess the ability of thermals to penetrate the inversion at the top of the boundary layer rather than basing the convective trigger solely on whether thermals can be expected to exist under given conditions.

The treatment of convective triggering by thermals described here attempts to account for the transition regime between free and forced convection, but the degree to which this transition is realistically represented is a subject for further investigation. Some preliminary (though indirect) support has been cited for the cloud-base mass flux scaling employed here based on trade wind region studies by LeMone and Pennell (1976) and Grossman (1982), and on a study by Moorthi and Suarez (1992) in which GATE data was used. Whether or not further research supports the present approach, identification of the transition regime in model simulations presents the opportunity, in principle, for further specialization of cumulus parameterization methods. Clouds that characteristically occur in this regime might be expected to differ in important respects from clouds occurring under free convective conditions.

Convective triggering in numerical models is closely tied with the closure used for the convective parameterization. Convective schemes with closures that are not based on buoyancy can be expected to exhibit different sensitivities than shown here. One may expect, for example, that a convective parameterization such as that of Tiedtke (1989), in which the cloud mass flux for penetrative convection and midlevel convection is determined by the large-scale moisture convergence, may not be as susceptible to producing excessive precipitation over the Pacific trade wind regions as found here. The reason is that the large-scale moisture convergence in the western Pacific appears to have a natural tendency to be concentrated over the warm pool region due to buoyancy and large-scale uplift associated with fluxes from the surface.

As discussed in section 3, the relatively low proportion (33% in EX1) of convective precipitation simulated over the Pacific warm pool RD region (boxed region in Fig. 2) in this study has caused some concern. Possible reasons for the apparent deficiency have been cited, including the failure of the present scheme to account for subgrid-scale variability, and the lack of a treatment for convection from elevated source levels. The problem does not occur when a standard entraining plume model (as opposed to the entraining–detraining model used here) is used in the NOGAPS RAS scheme, suggesting that the convective scheme used here may not be responding as it should to forcing in the region.

The performance of the present convective triggering parameterization is closely linked to the treatment of the atmospheric boundary layer. Simulated (EX1) boundary layer depths over the western Pacific in the present study averaged about 800 m, consistent with observations during the Tropical Ocean Global Atmosphere (TOGA) Coupled Ocean–Atmosphere Response Experiment (COARE) (Ding et al. 1995) in the east trade wind regime. Observations during TOGA COARE show considerable variability in boundary layer height associated with the occurrence of westerly wind burst episodes. The significant variations in SST that can occur during those episodes (Lin and Johnson 1996) have not been represented in the present (AGCM) tests. It seems likely that the present results may therefore not reflect some of the natural variability in boundary layer conditions in the tropical Pacific. The observed dominance of low-level winds as regards the determination of boundary layer regime in the present simulations (section 4) may thus be questionable. Further tests with coupled ocean–atmosphere models may be helpful in addressing this point.

The present work illustrates the importance for numerical simulation of the tropical Pacific climate of adequately treating the process of convective triggering. Nonetheless, it appears that some measure of success can be expected over the warm pool region from any scheme that can be adjusted so as to sufficiently limit convection along the ITCZ and in the northeast trade wind region. This point is demonstrated in experiments in which the low-level relative humidity threshold for deep convection in the NOGAPS AGCM is progressively increased. One finds that although warm pool precipitation can be effectively tuned using this method, there is a tendency toward excessive precipitation to the east of the Philipines and on the major islands of the Maritime Continent. The latter problem is common to many GCMs (Lau et al. 1996). A positive aspect of such a treatment is that it significantly reduces the overprediction of precipitation in the western Indian Ocean in

NOGAPS. Nonetheless, the triggering parameterization presented here appears to have a stronger physical basis, and further refinement should enhance its robustness under diverse conditions. Tests of the impact of the present scheme on the simulation of other seasons as well as intraseaonal variability is a subject of current investigation.

*Acknowledgments.* Support of the sponsors, Office of Naval Research Program Element 0601153N and Naval Research Laboratory Program Element 0602435N, is gratefully acknowledged. This work was supported in part by a grant of HPC time from the DoD HPC Shared Resource Centers, Army CEWES, Vicksburg, Mississippi, and NAVO Stennis Space Center, Bay St. Louis, Mississippi. Thanks go to S. Burk and J. Glendening for helpful discussions and to an anonymous reviewer for helpful comments on an earlier version of the manuscript.

## REFERENCES

Beljaars, A. C. M., 1994: The parameterization of surface fluxes in large-scale models under free convection. *Quart. J. Roy. Meteor. Soc.,* **122,** 255–270.

——, and A. A. M. Holtslag, 1991: Flux parameterization over land surfaces for atmospheric models. *J. Appl. Meteor.,* **30,** 327–341.

Bjerknes, J., 1969: Atmospheric teleconnections from the equatorial Pacific. *Mon. Wea. Rev.,* **97,** 163–172.

Charnock, H., 1955: Wind stress on a water surface. *Quart. J. Roy. Meteor. Soc.,* **81,** 639–640.

Davies, R., 1982: Documentation of the solar radiation parameterization in the GLAS climate model. NASA Tech. Memo 83961, 57 pp. [NTIS N82-30779/4.]

Deardorff, J. W., 1972: Numerical investigation of neutral and unstable planetary boundary layers. *J. Atmos. Sci.,* **29,** 91–115.

Ding, Y. H., A. Sumi, and X. S. Shen, 1995: Structures of the mixed layer and estimates of sea surface fluxes during TOGA-COARE IOP. Part I: Structures of the mixed layer. *J. Meteor. Soc. Japan,* **73,** 569–583.

Gates, W. L., 1992: AMIP: The Atmospheric Model Intercomparison Project. *Bull. Amer. Meteor. Soc.,* **73,** 1962–1970.

Grossman, R. L., 1982: An analysis of vertical velocity spectra obtained in the BOMEX fair-weather, trade-wind boundary layer. *Bound.-Layer Meteor.,* **23,** 323–357.

Harshvardhan, R. Davies, D. A. Randall, and T. G. Corsetti, 1987: A fast radiation parameterization for atmospheric circulation models. *J. Geophys. Res.,* **92,** 1009–1016.

Hogan, T. F., and T. E. Rosmond, 1991: The description of the Navy Operational Global Atmospheric Prediction System's Spectral Forecast Model. *Mon. Wea. Rev.,* **119,** 1786–1815.

——, and L. R. Brody, 1993: Sensitivity studies of the navy's Global Forecast Model parameterizations and evaluation of improvements to NOGAPS. *Mon. Wea. Rev.,* **121,** 2373–2395.

Holtslag, A. A. M., E. I. F. De Bruijn, and H.-L. Pan, 1990: A high resolution air mass transformation model for short-range weather forecasting. *Mon. Wea. Rev.,* **118,** 1561–1575.

Huang, R., and F. Sun, 1992: Impacts of the tropical western Pacific on the East Asian summer monsoon. *J. Meteor. Soc. Japan,* **70,** 243–256.

Kain, J. S., and J. M. Fritsch, 1992: The role of the convective ''trigger function'' in numerical forecasts of mesoscale convective systems. *Meteor. Atmos. Phys.,* **49,** 93–106.

Kuettner, J. P., 1959: The band structure of the atmosphere. *Tellus,* **11,** 267–294.

——, 1971: Cloud bands in the earth's atmosphere—Observations and theory. *Tellus,* **23,** 404–426.

Lau, K.-M., J. H. Kim, and Y. Sud, 1996: Intercomparison of hydrologic processes in AMIP GCMs. *Bull. Amer. Meteor. Soc.,* **77,** 2209–2227.

LeMone, M. A., and W. T. Pennell, 1976: The relationship of trade wind cumulus distribution to subcloud layer fluxes and structure. *Mon. Wea. Rev.,* **104,** 524–539.

Lin, X., and R. H. Johnson, 1996: Kinematic and thermodynamic characteristics of the flow over the western Pacific warm pool during TOGA COARE. *J. Atmos. Sci.,* **53,** 695–715.

Liu, G., J. A. Curry, and R.-S. Sheu, 1995: Classification of clouds over the western equatorial Pacific Ocean using combined infrared and microwave satellite data. *J. Geophys. Res.,* **100,** 13 811–13 826.

Louis, J. F., M. Tiedtke, and J. F. Geleyn, 1982: A short history of the operational PBL-parameterization at ECMWF. *Workshop on Boundary Layer Parameterization,* Reading, United Kingdom, ECMWF, 59–79.

McPhaden, M. J., and J. Picaut, 1990: El Niño–Southern Oscillation displacements of the western equatorial Pacific warm pool. *Science,* **250,** 1385–1388.

Mechoso, C. R., and Coauthors, 1995: The seasonal cycle over the tropical Pacific in coupled ocean–atmosphere general circulation models. *Mon. Wea. Rev.,* **123,** 2825–2838.

Moorthi, S., and M. J. Suarez, 1992: Relaxed Arakawa–Schubert: A parameterization of moist convection for general circulation models. *Mon. Wea. Rev.,* **120,** 978–1002.

Newell, R. E., 1979: Climate and the ocean. *Amer. Sci.,* **67,** 405–416.

Ramanathan, V., and W. Collins, 1991: Thermodynamic regulation of ocean warming by cirrus clouds deduced from observations of the 1987 El Niño. *Nature,* **351,** 27–32.

Ridout, J. A., B. Chertock, and R. Gelaro, 1994: The response of a GCM to a change in cloud solar forcing: Model feedbacks and comparison with satellite data. *J. Geophys. Res.,* **99,** 18 555–18 576.

Rogers, R. F., and J. M. Fritsch, 1996: A general framework for convective trigger functions. *Mon. Wea. Rev.,* **124,** 2438–2452.

Scorer, R., 1972: *Clouds of the World.* Stackpole Books, 176 pp.

Slingo, J., 1987: The development and verification of a cloud prediction scheme for the ECMWF model. *Quart. J. Roy. Meteor. Soc.,* **113,** 899–927.

Smith, S. D., 1980: Wind stress and heat flux over the ocean in gale force winds. *J. Phys. Oceanogr.,* **10,** 709–726.

——, 1988: Coefficients for sea surface wind stress, heat flux, and wind profiles as a function of wind speed and temperature. *J. Geophys. Res.,* **93,** 15 467–15 472.

Stull, R. B., 1988: *An Introduction to Boundary Layer Meteorology.* Kluwer Academic, 666 pp.

——, 1994: A convective transport theory of surface fluxes. *J. Atmos. Sci.,* **51,** 3–22.

Tiedtke, M., 1989: A comprehensive mass flux scheme for cumulus parameterization in large-scale models. *Mon. Wea. Rev.,* **117,** 1779–1800.

Troen, I., and L. Mahrt, 1986: A simple model of the atmospheric boundary layer; sensitivity to surface evaporation. *Bound.-Layer Meteor.,* **37,** 129–148.

Waliser, D. E., 1996: Formation and limiting mechanisms for very high sea surface temperature: Linking the dynamics and the thermodynamics. *J. Climate,* **9,** 161–188.

Webster, P. J., and R. Lukas, 1992: TOGA COARE: The Coupled Ocean–Atmosphere Response Experiment. *Bull. Amer. Meteor. Soc.,* **73,** 1377–1416.

Yanai, M., S. Esbensen, and J. H. Chu, 1973: Determination of the bulk properties of tropical cloud clusters from large-scale heat and moisture budgets. *J. Atmos. Sci.,* **30,** 611–627.